Available online at www.sciencedirect.com
ScienceDirect
Journal of Power Sources 164 (2007) 885–889
JOURNAL OF POWER SOURCES
www.elsevier.com/locate/jpowsour

Short communication

Morphology and electrochemistry of $LiMn_2O_4$ optimized by using different Mn-sources

Shu-Juan Bao [a], Chang-Ming Li [a,*], Hu-Lin Li [b], John H.T. Luong [c]

[a] *School of Chemical and Biomedical Engineering, Nanyang Technological University, Nanyang Avenue, Singapore 639798, Singapore*
[b] *College of Chemistry and Chemical Engineering, Lanzhou University, Lanzhou 730000, PR China*
[c] *National Research Council Canada, Biotechnology Research Institute, Montreal, Canada H4P2R2*

Received 2 August 2006; accepted 3 November 2006
Available online 14 December 2006

Abstract

Spinel-typed $LiMn_2O_4$ cathode active materials have been prepared for different microstructures by the melt-impregnation method using different forms of manganese. The effect of the starting materials on the microstructure and electrochemical properties of $LiMn_2O_4$ is investigated by X-ray diffraction, scanning electron microscopy, and electrochemical measurements. The powder prepared from nanostructured γ-MnOOH, with good crystallinity and a regular cubic spinel shape, provided an initial discharge capacity of 114 mAh g^{-1} with excellent rate and high capacity retention. These advantages render $LiMn_2O_4$ attractive for practical and large-scale applications in mobile equipment.

Keywords: Lithium-ion batteries; γ-MnOOH; $LiMn_2O_4$; Spinel-type; Discharge rate; Capacity retention

1. Introduction

Rechargeable lithium-ion batteries have become commercially feasible for diversified mobile electronic equipment. The market push for portable electronic devices creates a very strong driving force towards the development of light, efficient, environmentally friendly, and inexpensive rechargeable lithium-ion batteries [1,2]. The commonest cathode material, $LiCoO_2$, has good capacity and rechargeability, but suffers from the high cost and biotoxicity of cobalt [3]. Consequently, it is of importance to search for alternatives and the most promising materials are identified as $LiNiO_2$, $LiMn_2O_4$ and their related derivatives.

Intensive research has particularly focused on $LiMn_2O_4$ [4–6] because of the low cost and non-toxicity of manganese. Despite such merits, $LiMn_2O_4$ still has difficulty in practical applications, owing to its severe capacity depletion. Although the rationale behind the capacity loss is not completely understood, several contributing factors could include Jahn-Teller distortion, lattice instability, manganese dissolution, and electrolyte decomposition [4–8]. To overcome this problem, many methods for the cycleability improvement of spinel cathodes have been considered. One factor affecting the electrochemical behaviour, especially the capacity, is dependent on the microstructure of the resulting compounds [9]. The latter is determined by the structure and morphology of the starting materials, reaction temperature and time, and the preparation technique itself [10,11].

In this work, different compounds have been selected as a manganese source for the preparation and optimization of spinel-structured $LiMn_2O_4$. The physical characteristics and electrochemical properties of the synthesized products are presented and discussed.

2. Experimental

2.1. Preparation of γ-MnO_2

All the chemicals were of analytical grade and used without further purification. γ-MnO_2 powder was prepared as described elsewhere [12,13]. A solution (100 mL) consisting of 0.84 M $Na_2S_2O_8$ and 0.84 M $MnSO_4{\cdot}H_2O$ was heated to the boiling point for about 5 min, cooled, and filtered. The precipitate obtained, after thorough rinsing with deionized water until the resulting pH was near 7, was dried at 55 °C for 12 h.

* Corresponding author. Tel.: +65 67904485; fax: +65 67911761.
E-mail addresses: sjbao@ntu.edu.sg (S.-J. Bao), ecmli@ntu.edu.sg (C.-M. Li).

0378-7753/$ – see front matter © 2006 Elsevier B.V. All rights reserved.
doi:10.1016/j.jpowsour.2006.11.015

2.2. Preparation of γ-MnOOH

The aforementioned γ-MnO_2 (1 g) was added to 85 mL of 5% NH_4OH in a Teflon-lined 100 mL-capacity autoclave. After stirring for 1 min with a stainless-steel muddler, the autoclave was sealed and heated to 200 °C for 24 h. The system was then allowed to cool to room temperature. The collected product after filtration was washed with deionized water and dried at 55 °C.

2.3. Preparation of $LiMn_2O_4$ using EMD, γ-MnO_2 or γ-MnOOH

$LiMn_2O_4$ powder was synthesized by the melt-impregnation method. A stoichiometric amount of $LiNO_3$ and electrolytic manganese dioxide (EMD), γ-MnO_2 or γ-MnOOH was mixed by grinding. The obtained precursor was annealed at 260 °C for 4 h in air. After cooling and grinding, the precursor was calcined at 610 °C for 2 h and then at 750 °C for 12 h followed by slow cooling to room temperature.

2.4. Structure and morphology characterization

The crystal structure of the product was characterized by X-ray diffraction (XRD, D/max-2400 Rigaku, Japan) with Cu Kα radiation (λ = 1.54178 Å) operating at 50.0 kV and 200.0 mA. The morphology of the synthesized materials was investigated by scanning electron microscopy (SEM, JSM-5600LV, Japan).

2.5. Electrochemical measurements

Powder of the prepared cathode materials was mixed with 15 wt.% acetylene black. Polyvinylidene fluoride (5 wt.%, PVDF as binder, dissolved in *N*-methyl pyrrolidone), was added until a slurry solution was obtained. The slurry was pasted on aluminum foil followed by vacuum drying at 100 °C for 24 h. The cell consisted of a cathode, Li metal as an anode, and an electrolyte of 1 M LiPF6 in a 1:1 (v/v) mixture of ethylene carbonate (EC) and dimethyl carbonate (DMC). A Celgard 2400 membrane served as the cell separator. The assembly of the cell was conducted in an argon-filled glove-box. The cell was charged and discharged from 3.0 to 4.4 V at different current rates (Land CT2001A). Cyclic voltammetry was performed in the voltage range of 3.0–4.5 V at a scan rate of 0.1 mV s^{-1} using a CHI 760 Electrochemical Workstation (CH Instruments, Austin, TX).

3. Results and discussion

The XRD pattern of commercial EMD widely used in primary batteries displayed the characteristic peaks of γ-MnO_2, see curve (a), Fig. 1A. The broad and low-intensity peaks attested that EMD has a low degree of crystallization. The pattern in Fig. 1A (curve b) confirmed the formation of γ-MnO_2 (JCPDS no. 14-0644). All the diffraction peaks in Fig. 1A (curve c) could be readily indexed to a monoclinic phase of γ-MnOOH with lattice constants $a = 5.300$ Å, $b = 5.278$ Å and $c = 5.307$ Å, which agree with the literature values of JCPDS no. 41-1379.

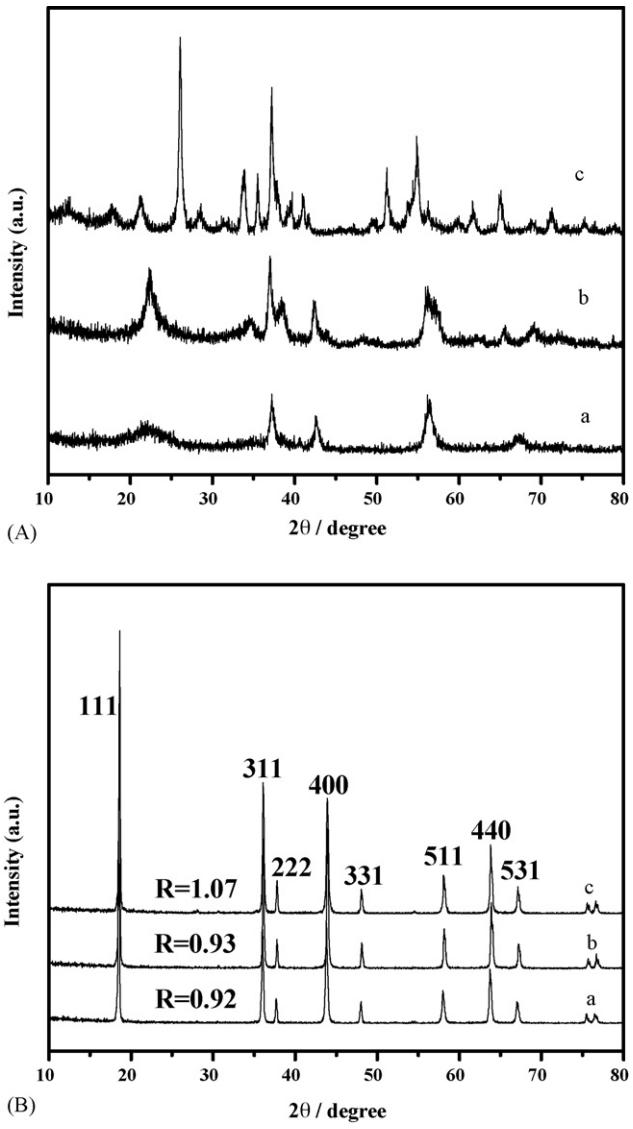

Fig. 1. (A) X-ray diffraction patterns of different manganese sources: curve a, EMD; curve b, γ-MnO_2; curve c, γ-MnOOH; (B) X-ray diffraction patterns of $LiMn_2O_4$ obtained by using different manganese sources: curve a, EMD; curve b, γ-MnO_2; curve c, γ-MnOOH. *R* is the intensity ratio of the (3 1 1)/(4 0 0) peaks.

Such results confirm that γ-MnO_2 is indeed transformed into γ-MnOOH during the hydrothermal process.

The XRD patterns of the spinel $LiMn_2O_4$ prepared from EMD, γ-MnO_2 and γ-MnOOH are presented in Fig. 1B. All the materials exhibit the same crystalline cubic spinel phase structure without any impurities and the results are in agreement with the standard spectra (JCPDS, card no. 89-0118). There are, however, some different characteristics among these manganese-based materials. These (3 1 1)/(4 0 0) peak intensity ratio (*R*), obtained for the samples prepared from γ-MnO_2 and EMD is 0.92 and 0.93, respectively. Such values are lower than that for the sample prepared from γ-MnOOH ($R = 1.07$). It should be noted that the shape of the (3 1 1)/(4 0 0) peaks reflects the degree of tetragonal distortion from the cubic spinel structure [10,14,15]. Therefore, the structural difference of $LiMn_2O_4$ pre-

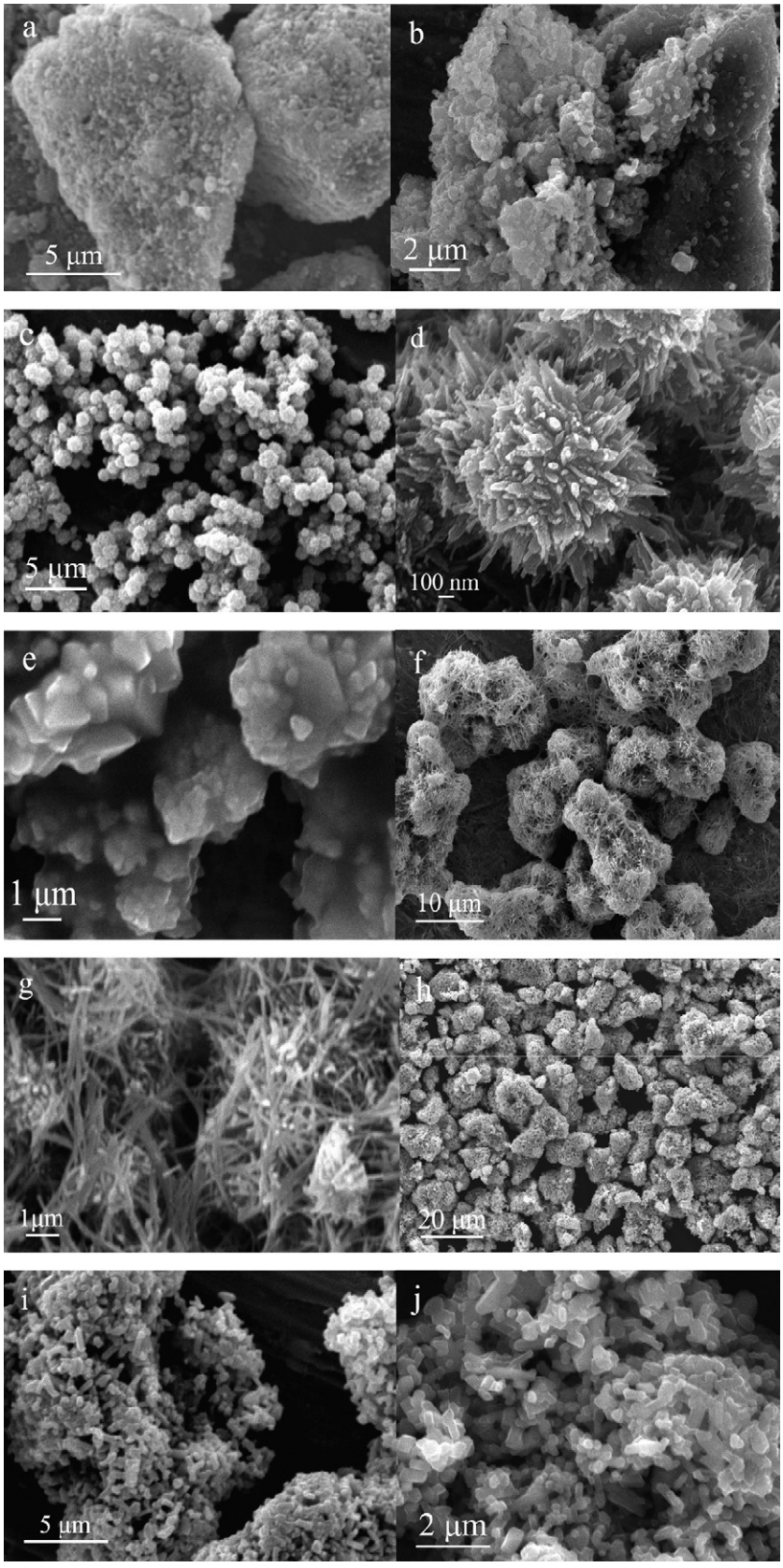

Fig. 2. Scanning electron micrographs: (a) EMD; (b) $LiMn_2O_4$ prepared from EMD source; (c) γ-MnO_2 with low magnification; (d) γ-MnO_2 with high magnification; (e) $LiMn_2O_4$ prepared from γ-MnO_2; (f) γ-MnOOH with low magnification; (g) γ-MnOOH with high magnification; (h) $LiMn_2O_4$ prepared from γ-MnOOH with low magnification; (i) $LiMn_2O_4$ prepared from γ-MnOOH with moderate magnification; (j) $LiMn_2O_4$ prepared from γ-MnOOH with high magnification.

pared from γ-MnOOH may result from the different synthetic conditions and starting materials.

The particle size and morphology of all the prepared samples were examined by SEM. Only irregular-shaped blocks are observed for EMD (Fig. 2a), whereas $LiMn_2O_4$ prepared from EMD (Fig. 2b) consists of a large number of small particles. These small particles, however, aggregated to form big blocks that resemble the fundamental shape of the starting material, EMD. The prepared γ-MnO_2 material consisted of small spherical particles (Fig. 2c) with irregular surfaces (Fig. 2d). Scanning election microscopic imaging for $LiMn_2O_4$ prepared from γ-MnO_2 revealed the formation of irregular particles with a broad particle size-distribution. Therefore, it is difficult to prepare regular and uniform $LiMn_2O_4$ powder from γ-MnO_2 as the precursor. Electron micrographs of γ-MnOOH prepared by the hydrothermal process are given in Fig. 2f–g. Although the γ-MnOOH particles are much larger, they still preserve the spherical structure of the starting material (γ-MnO_2) after the hydrothermal treatment. In addition, this material consists of a large quantity of wire-like nano-objects. The bird-nest morphology of γ-MnOOH enables easier and more homogenous impregnation of melted $LiNO_3$ into the porous structure. Therefore, it is interesting to examine the morphology of $LiMn_2O_4$ prepared from γ-MnOOH. At first glance, the material tends to form a loose, porous structure (Fig. 2h). Indeed, it is made up of small regular cubic, spinel-structured particles that agglomerate to form larger clusters (Fig. 2i and j). The surface area of the cluster-structured $LiMn_2O_4$ is higher than that of $LiMn_2O_4$ prepared from EMD or γ-MnO_2. The interconnected pores formed channels that allow the electrolyte to move into the electrode powder more freely. In other words, such morphology results in an increasing liquid|solid interfacial area and facilitates electrolyte diffusion. Consequently, this structure might be favourable for the insertion or extraction of lithium ions from the $LiMn_2O_4$ electrode.

3.1. Electrochemical properties

In order to study the influence of different manganese sources on the electrochemical performance of $LiMn_2O_4$, the cells were tested at a charge–discharge current density of 40 mA g^{-1} (C/3 rate) between 3.0 and 4.4 V. The variation of the discharge capacity with the cycle number for $LiMn_2O_4$ powder prepared using different manganese sources is shown in Fig. 3. Although the initial discharge capacitance among these cells is similar, after 30 cycles the discharge capacity of the $LiMn_2O_4$ prepared from γ-MnO_2 is relatively low and decreases rather rapidly. By contrast, the $LiMn_2O_4$ obtained from γ-MnOOH retains a higher capacity compared with its original charge value. The loose, porous, cluster-structured $LiMn_2O_4$ particles prepared from γ-MnOOH are expected to contribute to the good electrochemical performance of the material [9,16,17]. It has been reported that $LiMn_2O_4$ prepared from γ-MnOOH is composed of mixed cubic and tetragonal phases [10,14,15]. The tetragonal phase does not take part in the structural change during the charge–discharge process in the 3 V region. Therefore, it is likely that some of the tetragonal phase retains its original state and suppresses the

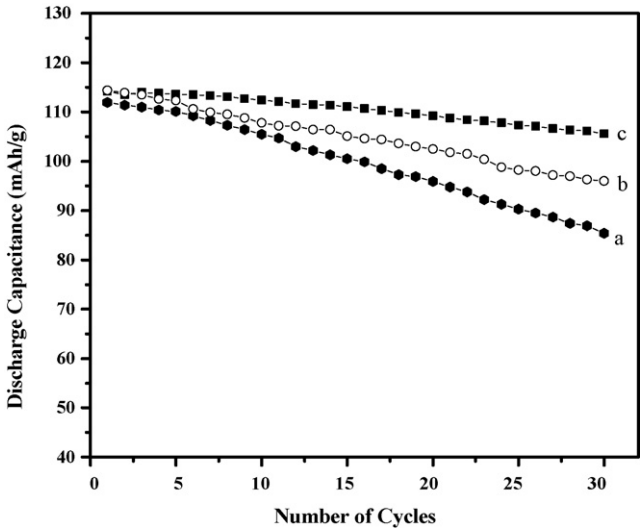

Fig. 3. Typical discharge capacity vs. the cycle number for $LiMn_2O_4$ prepared from (a) EMD; (b) γ-MnO_2; (c) γ-MnOOH.

spinel volume change during the intercalation–de-intercalation of lithium ions. The results presented here show that after 30 cycles, the material still displays a high discharge capacity, even with the Jahn-Teller distortion effect of the cubic phase. As such, γ-MnOOH may be a better alternative to traditional EMD as a manganese source for the preparation of spinel $LiMn_2O_4$ as a cathode material for lithium-ion batteries. As a consequence of this finding, further testing was focused on $LiMn_2O_4$ prepared from γ-MnOOH.

Fig. 4 displays the discharge capacity versus the cycle number for $LiMn_2O_4$ powder prepared from γ-MnOOH at different current rates (C/3, 2 C/3 and 1 C). All three curves indicate a good cycleability and a high-rate capability. The discharge capacity exhibits a slight tendency to decrease with increasing discharge current density. After 30 cycles, the 1 C discharge capacity is 94% of the discharge obtained for C/3. It is well known that a high-rate discharge capacity is one of the most important per-

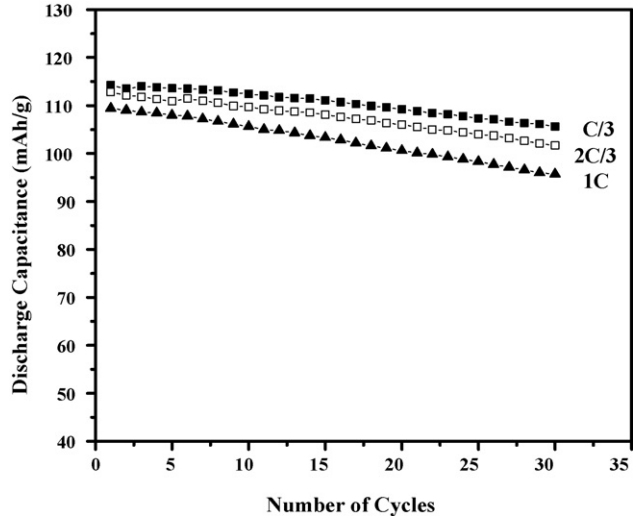

Fig. 4. Variations of discharge capacity with cycle number of $LiMn_2O_4$ prepared from γ-MnOOH at different charge–discharge rates.

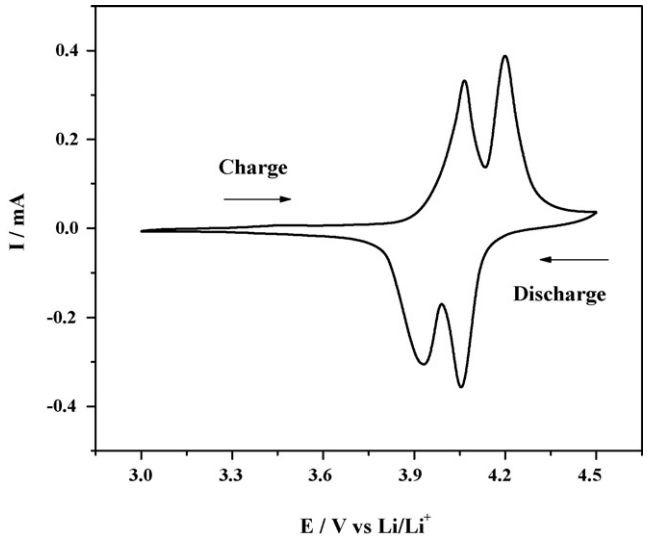

Fig. 5. Cyclic voltammogram of $LiMn_2O_4$ prepared from γ-MnOOH at a scan rate of 0.1 mV s^{-1}.

formance criteria for application as a battery electrode [18,19]. Therefore, the excellent rate capability of this sample makes it attractive for practical applications.

The cyclic voltammogram (CV) for $LiMn_2O_4$ prepared form γ-MnOOH is displayed in Fig. 5. The anodic and cathodic peaks observed in the CV of the $LiMn_2O_4$ powder indicate reversible oxidation and reduction that corresponds to lithium extraction and insertion. The split of the redox peaks into two couples shows that the electrochemical reaction of the insertion and extraction of Li ions occurred in two stages [20,21]. In spinel $LiMn_2O_4$, Li ions occupy tetrahedral sites (8a), Mn^{3+}, Mn^{4+} ions reside at the octahedral sites (16d), and O^{2-} ions are located at 32e sites [22]. The oxygen ions form a cubic closely packed array, tetrahedral sites (8a) share faces with vacant octahedral sites (16c), and thus form a three-dimensional vacant channel. Li ions intercalate or de-intercalate through these channels during the electrochemical reaction [23]. The first oxidation peak is attributed to Li ion removal from one-half of the tetrahedral sites. The second oxidation, the removal of Li ions from the remaining tetrahedral sites, can be described as follows [24]:

$$\frac{1}{2}Li^+ + \frac{1}{2}e^- + 2MnO_2 \Leftrightarrow Li_{0.5}Mn_2O_4 \quad (1)$$

$$\frac{1}{2}Li^+ + \frac{1}{2}e^- + Li_{0.5}Mn_2O_4 \Leftrightarrow LiMn_2O_4 \quad (2)$$

The redox peaks of the $LiMn_2O_4$ electrode are sharp with well-defined splitting, which indicates good crystallinity of the powder. The ratio for the two peak currents, ip_a/ip_c, is close to unity and, therefore, confirms the reversible intercalation and de-intercalation of Li ions in/from $LiMn_2O_4$; this is in agreement with the literature [25]. The present finding also reveals that $LiMn_2O_4$ possesses a structure that favours the transportation of Li ions.

4. Conclusions

Spinel-phased, well-crystallized $LiMn_2O_4$ powder has been synthesized by using γ-MnOOH as the manganese source. The material has a loose, porous, cluster-like structure that consists of small and regular particles, and that provides enhanced cycleability. The good cycleability and high-rate capability, coupled with the low cost and environmentally benign nature of manganese, render this material attractive for positive electrodes in lithium-ion batteries.

References

[1] J.M. Tarascon, M. Armand, Nature 414 (2001) 359.
[2] V. Ganesh Kumar, J.S. Ganaraj, S. Ben-David, D.M. Pickup, E.R.H. Van-Eck, A. Gedanken, D. Aurbach, Chem. Mater. 15 (2003) 4211.
[3] Y.K. Sun, C.S. Yoon, C.K. Kim, S.G. Youn, Y.S. Lee, M. Yoshio, I.H. Oh, J. Mater. Chem. 11 (2001) 2519.
[4] D.H. Jang, Y.J. Shin, S.M. Oh, J. Electrochem. Soc. 143 (1996) 2204.
[5] Y. Xia, Y. Zhou, M. Yoshio, J. Electrochem. Soc. 144 (1997) 2593.
[6] P. Arora, B.N. Popov, R.E. White, J. Electrochem. Soc. 145 (1998) 807.
[7] P.S. Whitfield, I.J. Davidson, J. Electrochem. Soc. 147 (2000) 4476.
[8] S.T. Myung, H.T. Chung, S. Komaba, N. Kumagai, H.B. Gu, J. Power Sources 90 (2000) 103.
[9] Y. Shin, A. Manthiram, J. Power Sources 126 (2004) 169.
[10] Y.S. Lee, C.S. Yoon, Y.K. Sun, M. Yoshio, Electrochem. Solid State Lett. 5 (2002) A1.
[11] W. Zhang, Y. Liu, Z. Yang, S. Tang, M. Chen, Solid State Commun. 131 (2004) 441.
[12] R. Patrice, L. Dupont, L. Aldon, J.C. Jumas, E. Wang, J.M. Tarascon, Chem. Mater. 16 (2004) 2772.
[13] E.I. Wang, W.L. Bowden, L. Lin, U.S. Patent 532,584 (1996).
[14] M. Tabuchi, C. Masquelier, H. Kobayashi, R. Kanno, Y. Kobasashi, T. Akai, Y. Maki, H. Kageyama, O. Nakamura, J. Power Sources 68 (1997).
[15] M.M. Thackeray, Prog. Solid State Chem. 25 (1997).
[16] S.T. Yang, Y.F. Zhang, Q.Z. Lv, J. Inorg. Mater. 15 (2000) 312.
[17] F.K. Shokoohi, J.M. Tarascon, B.J. Wilkens, D. Guyomard, C.C. Chang, J. Electrochem. Soc. 139 (1992) 1847.
[18] S.H. Ye, J.Y. Lv, X.P. Gao, F. Wu, D.Y. Song, Electrochim. Acta 49 (2004) 1623.
[19] W.J. Zhou, S.J. Bao, B.L. He, Y.Y. Liang, H.L. Li, Electrochim. Acta 51 (2006) 4701.
[20] X.M. Wu, X.H. Li, Z.B. Xiao, J.B. Liu, W.B. Yan, M.Y. Ma, Mater. Chem. Phys. 84 (2004) 182.
[21] Y. Xia, M. Yoshio, J. Electrochem. Soc. 143 (1996) 825.
[22] S.S. Zhang, K. Xu, T.R. Jow, Electrochim. Acta 49 (2004) 1057.
[23] N. Santander, S.R. Das, S.B. Majumder, R.S. Katiyar, Surf. Coat. Technol. 177/178 (2004) 60.
[24] M. Armand, F. Dalard, D. Reroo, C. Mouliom, Solid State Ionics 15 (1985) 205.
[25] Y.Y. Xia, H. Takeshige, H. Noguchi, M. Yoshio, J. Power Sources 56 (1995) 61.